Lawrence Berkeley National Laboratory
LBL Publications

Title

Underwater unexploded ordnance discrimination based on intrinsic target polarizabilities — A case study

Permalink

Authors

Gasperikova, Erika

Conti, Ugo

Morrison, H Frank

Publication Date

DOI

Copyright Information

Peer reviewed

ORIGINAL ARTICLE

Geophysical Prospecting   EAGE   EUROPEAN ASSOCIATION OF GEOSCIENTISTS & ENGINEERS

Underwater unexploded ordnance discrimination based on intrinsic target polarizabilities – A case study

Erika Gasperikova[1] | Ugo Conti[2] | H. Frank Morrison[3]

[1]Lawrence Berkeley National Laboratory, Berkeley, California, USA

[2]Marine Advanced Robotics, Inc., Richmond, California, USA

[3]P. Malozemoff Professor Emeritus, University of California, Berkeley, California, USA

Correspondence
Erika Gasperikova, Lawrence Berkeley National Laboratory, One Cyclotron Road, Mail Stop 74R316C, Berkeley, CA 94720, USA.
Email: egasperikova@lbl.gov

Abstract

Seabed unexploded ordnance that resulted partly from the high failure rate among munitions from more than 80 years ago and from decades of military training and testing of weapons systems poses an increasing concern all around the world. Although existing magnetic systems can detect clusters of debris, they are not able to tell whether a munition is still intact requiring special removal (e.g. in situ detonation) or is harmless scrap metal. The marine environment poses unique challenges, and transferring knowledge and approaches from land to a marine environment has not been easy and straightforward. On land, the background soil conductivity is much lower than the conductivity of the unexploded ordnance and the electromagnetic response of a target is essentially the same as that in free space. For those frequencies required for target characterization in the marine environment, the seawater response must be accounted for and removed from the measurements. The system developed for this study uses fields from three orthogonal transmitters to illuminate the target and four three-component receivers to measure the signal arranged in a configuration that inherently cancels the system's response due to the enclosing seawater, the sea–bottom interface and the air–sea interface for shallow deployments. The system was tested as a cued system on land and underwater in San Francisco Bay – it was mounted on a simple platform on top of a support structure that extended 1 m below and allowed the diver to place metal objects to a specific location even in low-visibility conditions. The measurements were stable and repeatable. Furthermore, target responses estimated from marine measurements matched those from land acquisition, confirming that the seawater and air–sea interface responses were removed successfully. Thirty-six channels of normalized induction responses were used for the classification, which was done by estimating the target principal dipole polarizabilities. Our results demonstrated that the system can resolve the intrinsic polarizabilities of the target, with clear distinctions between those of symmetric intact unexploded ordnance and irregular scrap metal. The prototype system was able to classify an object based on its size, shape and metal content and correctly estimate its location and orientation.

INTRODUCTION

Unexploded ordnance (UXO), resulting partly from the high rate of failure among munitions from more than 80–100 years ago, presents serious problems in Europe, Asia and the United States. Areas of millions of square kilometres host underwater UXO. The US Army Corps of Engineers and the US Navy have identified over 400 underwater formerly used defence sites (e.g. DiMarco et al., 2010) that contain munitions or UXO over 40,000 km^2 area in less than 40 m of water. Around 1.6 million tons of conventional and 5000 t of chemical munitions were estimated to remain at over 71 munitions-contaminated sites in German waters alone (Böttcher et al., 2011).

UXO detection and discrimination using electromagnetic induction (EMI) systems on land have successfully been demonstrated (e.g. Beran et al., 2011; Billings et al., 2010; Gasperikova et al., 2009a, 2009b; Prouty et al., 2011; Shubitidze et al., 2014, 2021a; Song et al., 2012, 2013). The marine environment poses additional challenges related to the nature of the seawater environment and deployment. Therefore, transferring the knowledge and approaches on land to a marine environment has not been straightforward. Characterization and remediation of underwater sites are more expensive than land sites. Current technologies allow for the detection of metallic objects in the underwater environment, but divers perform characterization by manual inspection, which is expensive and time-consuming (e.g. Schultz, 2016). Only about 6% of the investigated targets are identified as UXO during UXO clearance campaigns (e.g. Guldin, 2021). State-of-the-art UXO detection methods in marine environments include ship-towed magnetometer arrays, side-scan sonar, multibeam echosounder and subbottom profiler (Frey, 2020; Wehner & Frey, 2022). After creating a map of potentially hazardous targets, these targets need to be characterized and classified as UXO or non-UXO, where EMI systems play an important role.

The ability to detect and discriminate UXO from non-UXO targets using EMI systems in marine environments depends on advances in two main areas: (1) reliable deployment and accurate system positioning and (2) accurate estimation of target properties and subsequent discrimination. The ability to deploy and collect data in various marine environments has been demonstrated with several prototype systems (e.g. Billings 2020; Funk et al., 2022; Miller et al. 2018, 2019; Schultz et al., 2021; Shubitidze et al. 2021a). One approach that can lead to successful target characterization is modelling the electromagnetic (EM) response of the complex marine environment and subtracting that from the total measured signals during data processing (e.g. Keranen et al. 2018; Kulgemeyer et al. 2019; Miller et al. 2021; Schultz et al. 2021; Shubitidze et al. 2021b; Song et al. 2021).

An alternative approach is to design a system configuration that would inherently eliminate the effect of marine conductive environment in hardware and increase sensitivity to metallic targets of interest. The seawater response is comparable to, or larger than, the response of the target. The system of measuring the differences of receivers placed symmetrically on either side of the transmitters cancels the seawater response because the induced currents in the seawater are also symmetric with respect to the transmitters. For symmetrically placed identical induction receiver coils, wired in opposition, the output voltage is zero during the primary field pulse in free-space, and at all times in a uniform conducting medium or in the vicinity of parallel plane interfaces in the plane of the transmitter and receiver. When a conducting object is near one of the receivers, the output is nonzero and proportional to the difference of the object's secondary field at the two receivers. Morisson (2013) described in detail the treatment of this problem and the hardware configuration that cancels the effects of the seawater and the air–sea interface. We present results demonstrating that such an approach is viable in achieving the desired performance. A marine version of the Berkeley UXO discriminator (MBUD), time-domain EM system, was designed and built to address these challenges and classify targets from a single system position to a depth of about 1.2 m.

For the rest of the paper, we first describe the acquisition system and discrimination approach. Then, we demonstrate a cued mode acquisition and object classification during field land and marine experiments in San Francisco Bay, CA and provide results comparison and system performance assessment.

INSTRUMENTATION

Two main parameters, the size of the transmitter and sensor array dimensions, control the system's capabilities. The field strength at depth depends on the dimensions of the transmitter, and the receiver spacing governs the depth estimates' accuracy. A simple 2.5 × 1.2 m^2 platform supports an open-frame electromagnetic (EM) prototype system consisting of three orthogonal transmitters at the centre and four three-component receiver cubes at the corners of a 1-m^2 area (Figure 1). The system uses a 5.0 ms bipolar half-sine pulse current waveform, and measurements are made in the
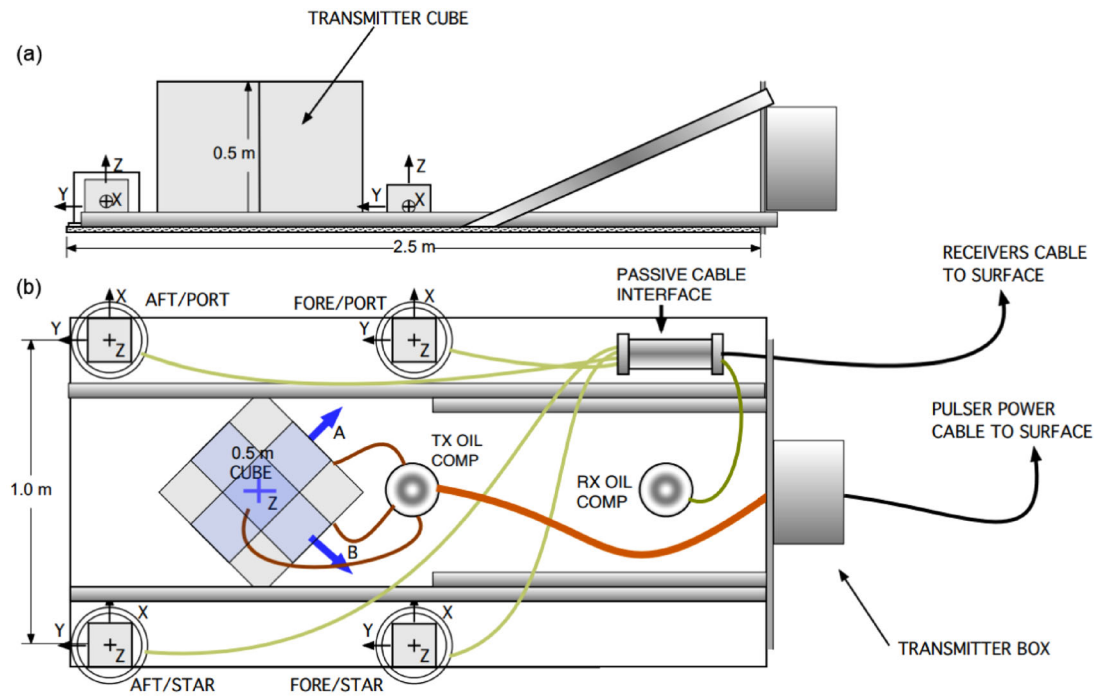
FIGURE 1 System configuration schematic: (a) side view and (b) plane view. The supporting platform is 2.5×1.2 m^2. Three-component receiver cubes are 1 m apart in a square pattern at the left end of the platform. A 0.5-m transmitter cube is at the centre of the receiver cubes. A, B and Z indicate three orthogonal transmitter coils. The transmitter electronics and power units are at the right end of the platform.

transmitter off-time. The pulser provides a peak moment of 2000 A-turns-m^2 with current pulses of 200 A and a net power consumption of 400 W. Differences in field at symmetrically positioned receivers cancel the seawater response and the air–sea interface for shallow deployments. The pulser and electronics inside the pressure casing are 2.0 m away from the transmitter cube centre at the end of the platform. Next to the transmitter electronics is also a dedicated pressure casing, inside of which all the signal and power connections are redistributed inside of a tether cable that reaches the surface vessel where the data are acquired, processed and analysed.

The orthogonal transmitter coil system is completely encased in epoxy glass composite to avoid any possibility of creating contact between seawater and the transmitter coil windings. The pressure-compensating oil filling system and wet pluggable high-pressure connectors are used for receiver and transmitter cables. Each three-component receiver and amplifier system are housed in a plastic cube 0.15 m on a side and enclosed in a plastic pressure case. Four three-component receivers are symmetrically placed on a horizontal plane around a three-component transmitter cube (Figure 1). Diametrically symmetric receivers see the same response from the seawater and from the horizontal air–sea interface, and both responses are cancelled in the difference. In some cases, the receiver outputs of a particular pair for one transmitter coil are of the same sign and must be differenced by the acquisition; for another coil, they are of opposite sign and must be summed, which is handled by the field-programmable

gate array (FPGA) board. The control system consists of two FPGA boards. The first board sends an acquisition sequence to the pulser in the pressure casing. The board is enclosed in a metal box to shield the high EM fields generated by the power switching from interfering with acquisition board operation. The second FPGA board that performs data acquisition and is connected through a connection box to the receivers' channels is on the service boat. The acquisition software developed for the Berkeley unexploded ordnance discriminator systems (e.g. Gasperikova et al., 2009a; Gasperikova et al., 2012) was modified for this system.

The system components are mounted on the top platform (Figure 2). The support structure extends 1 m below the system platform and allows for the object placement to a specific location and orientation. Four people easily handle the system. Two plates with uniform openings distribution centred below the transmitter cube centre allow for an accurate object position with respect to the system's centre, even in low-visibility conditions that might be encountered during underwater surveys.

OBJECT IDENTIFICATION

The induced moment of a target depends on the strength of the transmitted electromagnetic-inducing field. If we normalize the moment by the inducing field, we obtain polarizability. The secondary fields, measured as a function of time,

FIGURE 2 Marine system for a cued mode operation during land testing.

are related to the induced polarizabilities. The polarizabilities and their variation with time are the only fundamental object parameters that can be recovered from the inductive excitation of a finite body in the ground if a dipolar representation is assumed. Smith and Morrison (2004) were the first to introduce a satisfactory classification scheme based on the use of the principal dipole polarizabilities of a target. It has been demonstrated that a set of the intrinsic principal dipole polarizabilities of a target is key in discriminating unexploded ordnance (UXO) from irregular scrap metal (e.g. Gasperikova, et al., 2009a; Pasion et al. 2007; Prouty et al. 2011). Although other object identification approaches have been developed, the basic polarizability-based UXO classification methodologies are most frequently used and have been adopted by the US Department of Defense Advanced Geophysical Classification Accreditation Program to standardize the classification methodology (EPA, 2016). For a near-intact UXO, a major polarizability coincides with the object's long axis and two equal transverse polarizabilities (Figure 3a) in the direction of the minor axes. In comparison, scrap metal exhibits three distinct principal polarizabilities (Figure 3b). There are clear distinctions between symmetric intact UXO and irregular scrap metal. Because UXOs have unique polarizabilities, distinct individual signatures can distinguish each type of UXO. If uniform field illumination and dipole approximation are valid, these polarizability responses are independent of the target position and orientation. The distance at which this condition happens depends on the object's size. For large objects close to the system, higher order (non-dipole) terms are present due to source-field gradients along the length of the objects, which affect object orientation and equivalent dipole polarizability estimates. The discrimination software based on these properties developed

for the Berkeley unexploded ordnance discriminator systems (e.g., Gasperikova et al., 2012; Gasperikova et al., 2009b; Gasperikova, et al., 2009a) was adapted for this system.

FIELD SURVEYS AND RESULTS

Land tests

The tests on land were done at the University of California Richmond Field Station (UCRFS), California. Stability and repeatability are important parameters of the system's performance. The stability of the background transient is measured by differencing two background transients, and this is shown in Figure 4 at the start (Figure 4a) and at the end (Figure 4b) of the test, respectively. The upper, middle and lower panels show responses measured on 12 channels (c1–c12) for x, y and z transmitters, respectively. Each channel's small magnitude random variation defines the combined system and site noise level. Figure 4 illustrates that the system was stable, and measurements were repeatable. When a target was present (Figure 4c), the response was an order of magnitude larger and showed a typical decay response that enabled reliable object characterization. The background response (Figure 4a,b) was considered the system and the site calibration response, and it was subtracted from the measured response, allowing a 1:1 comparison of the measurements and results from different field sites. This was especially important for the measurements at the UCRFS, where variable high-level cultural noise was present. Figure 5 shows objects used for performance testing – 152-mm shotput, steel and aluminium 230-mm spheroids, 60-mm mortar, 70-mm rocket, 105-mm projectile, an anchor, two different size propellers, a
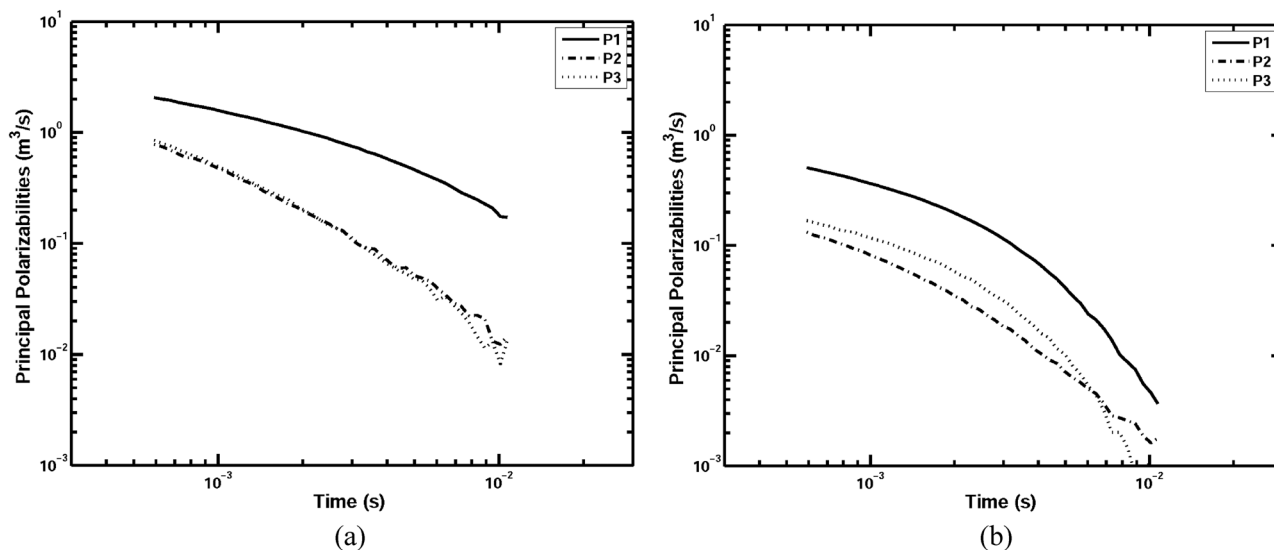
FIGURE 3 Inversion results for the principal polarizabilities of (a) 105 mm projectile and (b) scrap metal.
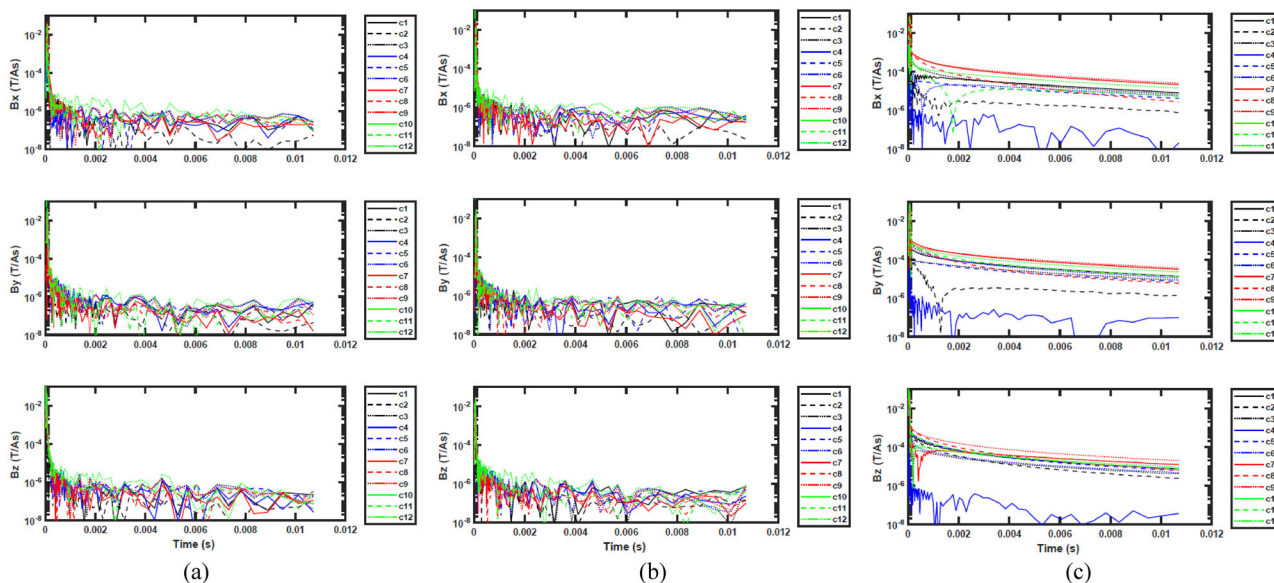

FIGURE 4 (a) Background response at the test start, (b) background response at the test end and (c) target response. Each panel represents one transmitter (x, y or z) and responses are measured on 12 channels (c1–c12).

chain and a piece of scrap metal. The target response depends on the target's size and depth, for example a shallow 152-mm shotput response was ~50 times above the background response, whereas when deep, the signal was only ~10 times larger than the background response. Similar signals were observed for the 105-mm projectile, over 100 times larger than the background for medium depths and only ~10 times above the background for the deepest location tested.

Following Gasperikova et al. (2009a), the principal dipole polarizabilities of a target were estimated from normalized induction responses in 36 channels and computed at 46 logarithmically spaced discrete times between 0.0005 and 0.013 s

after the turnoff. The background reference sounding taken within 30–40 min of the measurement, without any object present, was subtracted from a sounding for each object at various positions and orientations, inverted for principal polarizabilities, and inversion results were displayed on the computer screen. Intrinsic polarizability responses of selected targets are shown in Figure 6. Figure 7 shows that object locations were estimated within a few centimetres of the measured values. Figure 7d shows that over 90% of objects had location estimates better than 0.06 m. If the objects outside the system footprint were not included, this number would be 98%. In Figure 7d, the black symbols and left axis

FIGURE 5 Objects used for system testing: (1) 60-mm mortar, (2) chain, (3) a piece of scrap metal, (4) 230-mm spheroid, (5) 152-mm shotput, (6) 105-mm projectile, (7) 70-mm rocket, (8) large propeller, (9) anchor and (10) small propeller.

show location differences in depth, and the grey symbols and right axis show these differences for y-coordinates, both as a function of differences in x-coordinates on the horizontal axis. The excellent performance and discrimination capabilities of the system are illustrated by the 70-mm (2.75-in) rocket and 152-mm steel shotput, both clearly characterized down to 0.7 m and with the 105-mm projectile characterized down to a depth of 1.0 m. Figure 7e reveals that the system can discriminate objects to depths ~10 times the object's diameter. The 70-mm rocket was correctly characterized even when located 0.2 m outside the system footprint. For the 105-mm projectile located 0.2 m outside the system footprint (Figure 7b, solid circle at (−0.15, 0.7 m), depth and polarizabilities were correctly estimated, but estimates in y-location were 0.12–0.17 m from the measured location. During a field survey, for objects outside of the system footprint, the system would be moved closer, and measurements and classification repeated to ensure the correct location and characterization of the target. Scrap and non-unexploded ordnance (UXO) objects had responses that were different from those of UXO.

Marine tests

The underwater tests were performed in Richmond Marina Bay Yacht Harbor. The area is filled with 'bay mud', a soft unconsolidated silty clay. The water depth in the marina varies from 1.0 to 6.0 m. The measurements were done in an area with a water depth of 6.0 m. The marine UXO system can easily be transported and deployed using a carrier pontoon boat with two inflatable sides and a gantry crane capable of

carrying payloads similar to the system weight (Figure 8a). This boat is suitable for shallow or deep-water deployments.

The system was lowered into the water (Figure 8b) after a preliminary noise test in the air at the test location. Easy underwater handling by the diver was included in the design, as the system's buoyancy reduces the apparent weight. With the device on the sea bottom, the diver detached the winch cables, and the carrier boat was moved away from the test site. The underwater system was connected with a tether cable that includes both signal and power cables to the pulser high current, low voltage DC source, and the data acquisition system that resides on a service boat (operator's vessel). The system was operated from a computer on the service boat.

Figure 9 shows the background responses at the start (Figure 9a) and end (Figure 9b) of the test, respectively. Analogous to the land tests, the figure illustrates that the system was stable, measurements were repeatable and the noise level was much lower than the target response shown in Figure 9c. Again, the upper, middle and lower panels show responses measured on 12 channels (c1–c12) for x, y and z transmitters. The background noise level was 10–30 times lower than the one during our land tests (Figures 4a,b), as there was no industrial noise present as encountered at the Richmond Field Station. When the target is present (Figure 9c), the response is an order of magnitude larger and again shows the characteristic response decay. Because of lower background noise levels, the shallow 152-mm shotput response was ~50–100 times above the background response, whereas when located deep, the signal was ~20 times the background response. Signal levels of an aluminium spheroid, 60-mm projectile and 105-mm projectile were 7–30, 60 and over 200 times larger than the background.

The system was operated in a cued mode. We acquired data over typical marine UXO targets and scrap, that is a 152-mm shotput, 230-mm steel and aluminium spheroids, 60-mm mortar, 70-mm rocket, 105-mm projectile, anchor and a piece of scrap, at multiple positions and orientations. The device support structure described earlier allowed the diver to accurately place the object into a specified position and orientation with respect to the centre of the system (Figure 8c). Soundings were collected for each object and position, differenced with background reference soundings taken within 30–40 min of the measurement, without any metallic object present, and inversion results were displayed on the computer screen, including the object's estimated position and orientation. Although this was still a two-step process – the data acquisition was separate from the data processing and inversion, it allowed for real-time data quality checks on the service boat. Similar to land experiments, the principal dipole polarizabilities of a target (Figure 10) were estimated using 36 channels of normalized induction responses and calculated at 46 logarithmically spaced discrete times between 0.0005 and 0.013 s after the transient shutoff. Figure 11 shows the
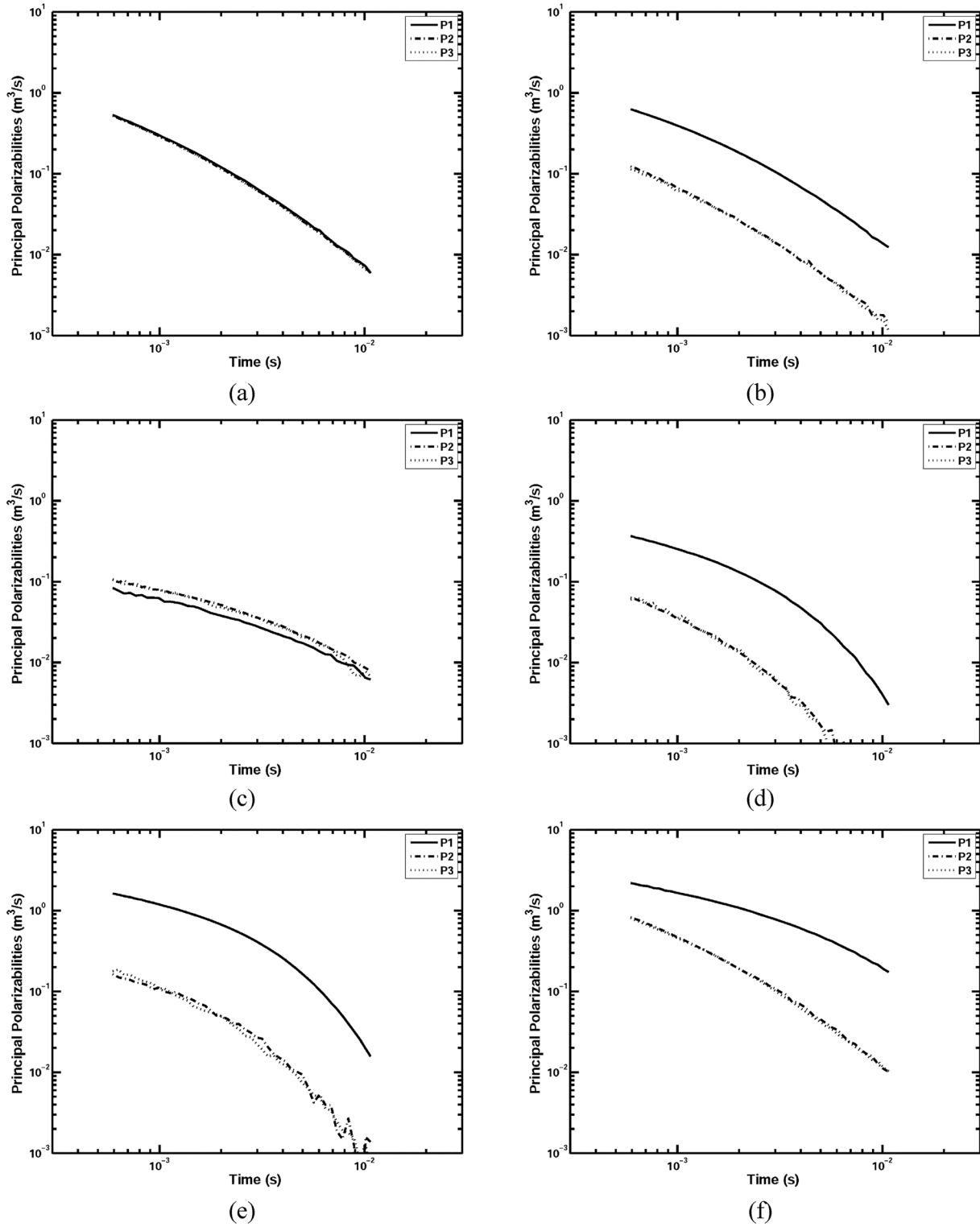
FIGURE 6 Principal polarizabilities as a function of time for (a) 152-mm shotput, (b) 230-mm steel spheroid, (c) 230-mm aluminium spheroid, (d) 60-mm mortar, (e) 70-mm rocket, (f) 105-mm projectile, (g) anchor, (h) chain, (i) propeller and (j) scrap metal.
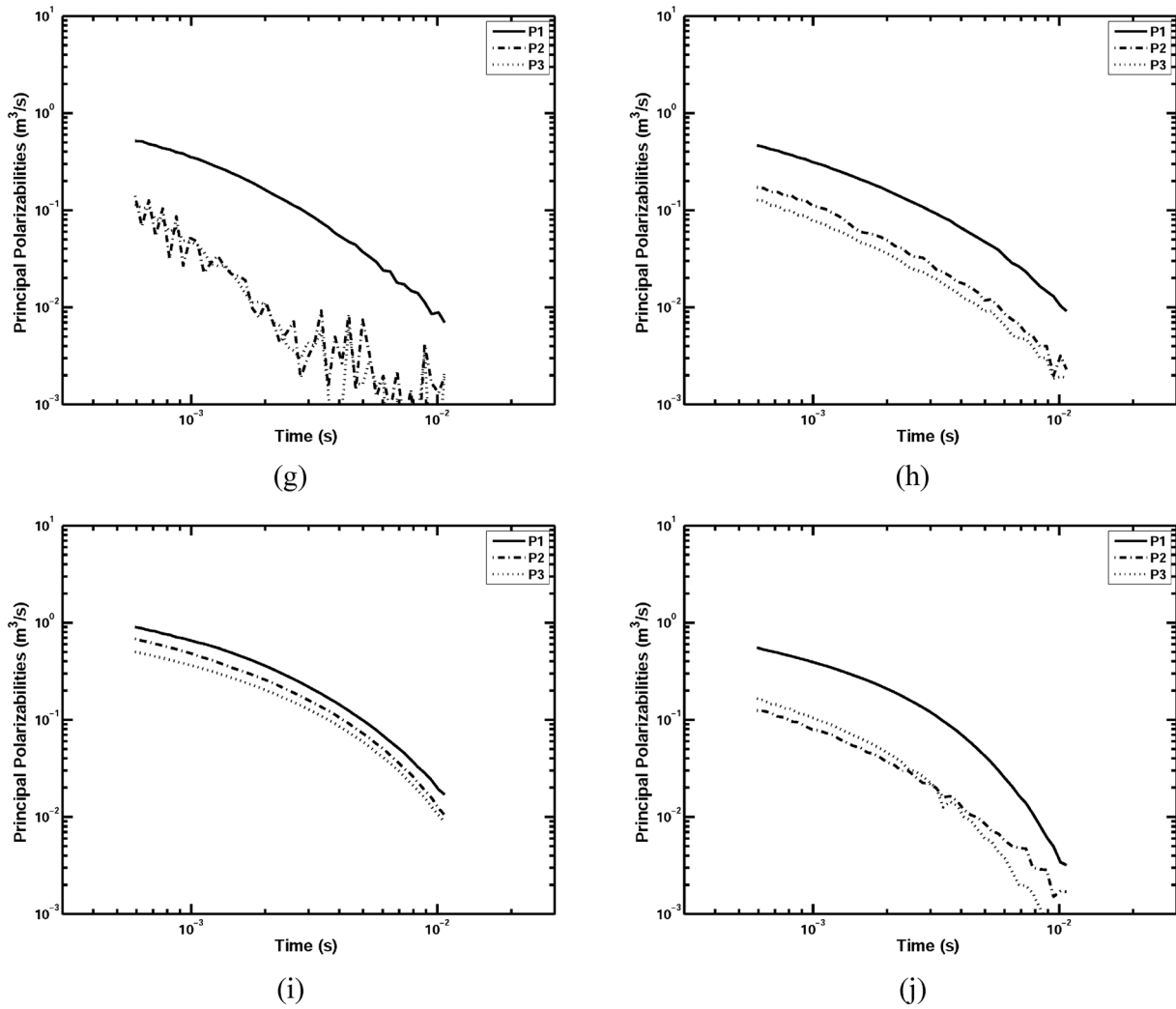
FIGURE 6 Continued

actual and estimated objects' depth and horizontal location relative to the centre of the transmitter cube by the inversion. Again, Figure 11d shows that the difference between measured and estimated locations was better than 0.05 m for over 90% of the objects. The 152-mm shotput was characterized 1.0 m away from the system, although the response was noisier (Figure 10b) than when the object was 0.5 m away from the system (Figure 10a). Figure 11e demonstrates that the system can discriminate objects to depths 10–11 times the object's diameter. The system discrimination capability based on a metal type is illustrated using 230-mm steel (Figure 10c) and aluminium (Figure 10d) spheroids. Polarizability responses produced by objects of the same size and shape but made from different materials are characteristically different. The response of aluminium spheroid (Figure 10d) is smaller in amplitude and has a slower decay with time; hence, polarizability curves have different shapes than those for steel spheroid (Figure 10c).

The results from underwater tests compare very well with the land test results. Figure 12 shows responses from both tests for the 60-mm mortar (Figure 12a), 70-mm rocket (Figure 12b), 105-mm projectile (Figure 12c) and 230-mm steel spheroid (Figure 12d). The results from underwater tests are plotted in grey, whereas the land results are plotted in black. Target responses estimated from marine measurements are within 10% of those from land measurements. The larger discrepancies and noise are present at late times when signals are small.

DISCUSSION AND CONCLUSIONS

These results demonstrate that the same discrimination capabilities of land electromagnetic induction systems are achievable in marine environments. Future work needs to address various survey modalities and deployments. Suppose
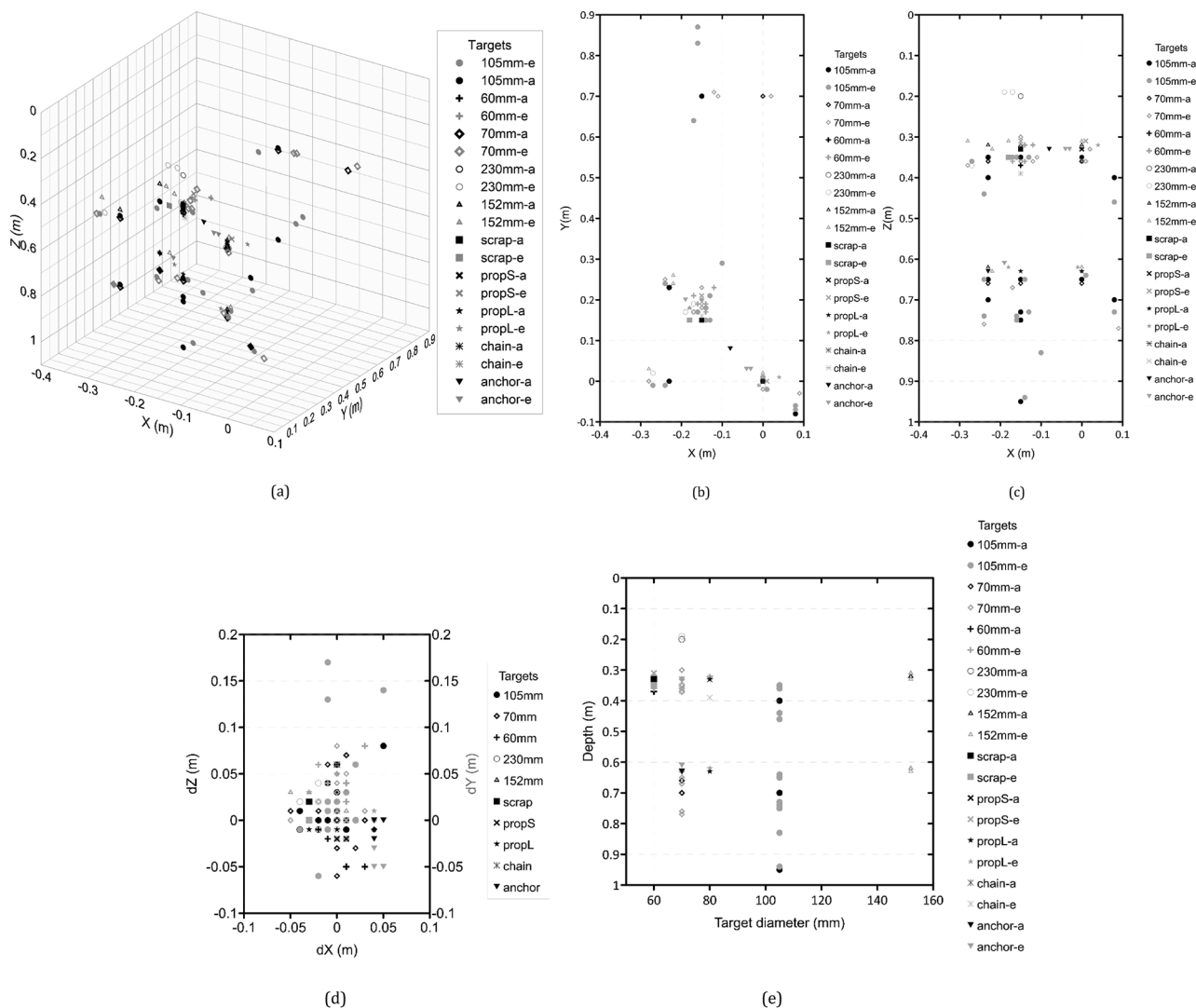
Geophysical Prospecting

EAGE
EUROPEAN
ASSOCIATION OF
GEOSCIENTISTS &
ENGINEERS

9

FIGURE 7 Actual (black symbols, a) and estimated (grey symbols, e) object locations in land experiment. (a) 3D view, (b) *XY* locations, (c) *XZ* locations, (d) differences between actual and estimated values and (e) target depths as a function of a target diameter. Test targets were 105-mm projectile, 60-mm mortar, 70-mm rocket, 230-mm steel and aluminium spheroids, 152-mm shotput, a piece of scrap metal, large (L) and small (S) propellers, chain and anchor.

a detection system locates targets in the area of interest. In that case, this system can navigate to those locations and identify the target based on acquired data in a stationary position and subsequent inversion. Another option is that the system would be used for both detection and discrimination in one survey, similar to what was demonstrated with land systems (e.g. Gasperikova et al., 2009a; Gasperikova et al., 2009b) or other marine systems (e.g. Billings, 2020; Miller et al., 2018). This is a challenging problem, as navigation, towing or mounting the system on a remotely operated vehicle needs to be implemented and tested in various marine environments. However, systems used in testing these functionalities (e.g. navigation, deployment) have dimensions comparable to ours, so one can leverage the latest technologies in such a system. With the ability to subtract external signals in hardware, our system

offers an alternative to those that rely on precise modeling of the entire system and environment. The discrimination capabilities can be improved by modifying the inversion code to allow for multi-object solutions for cases when multiple objects are close to each other. The survey objective and costs determine which form factor or modality best suits a particular marine environment. Single-pass systems (e.g. Funk et al. 2022) might be the most efficient for large areas and rough deep-sea deployment. Smaller systems like the one presented in this study might be most suitable for smaller areas or areas with difficult access.

The marine UXO system was tested on land and in San Francisco Bay at a water depth of 6.0 m in the cued mode. These experiments in a shallow marine environment demonstrated that the system response to enclosing seawater and the
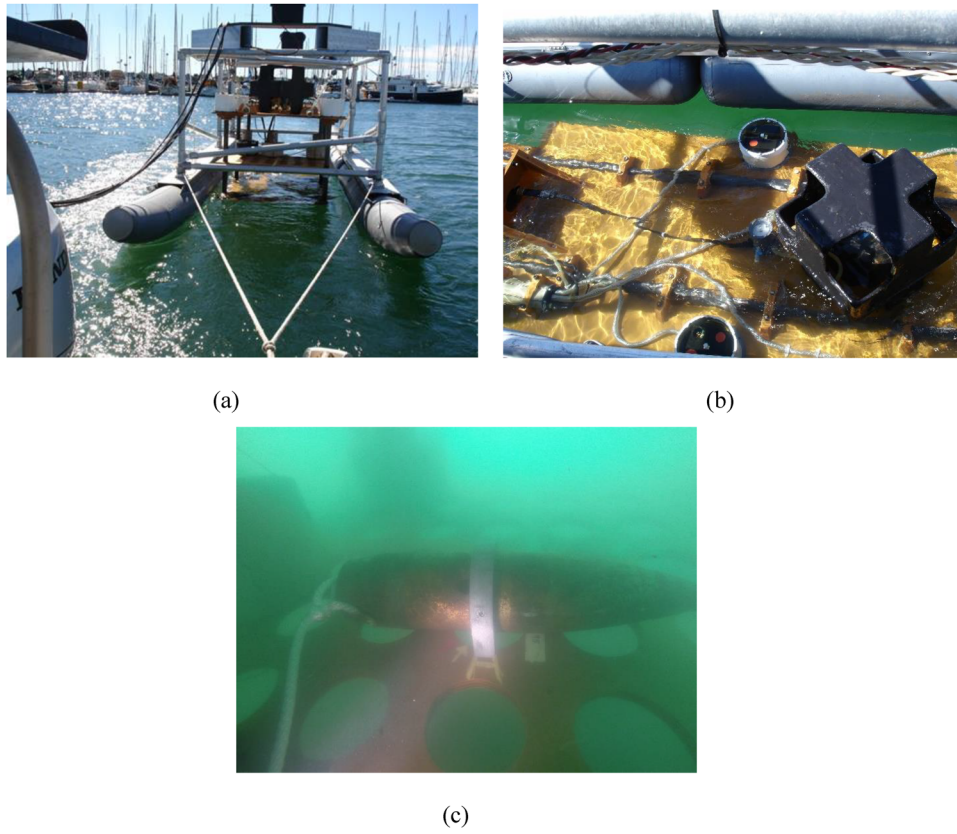
FIGURE 8   (a) The system transportation between the dock to the test site using the carrier boat towed behind the operator vessel, (b) lowering the system to the sea bottom and (c) object placement in a marine environment.
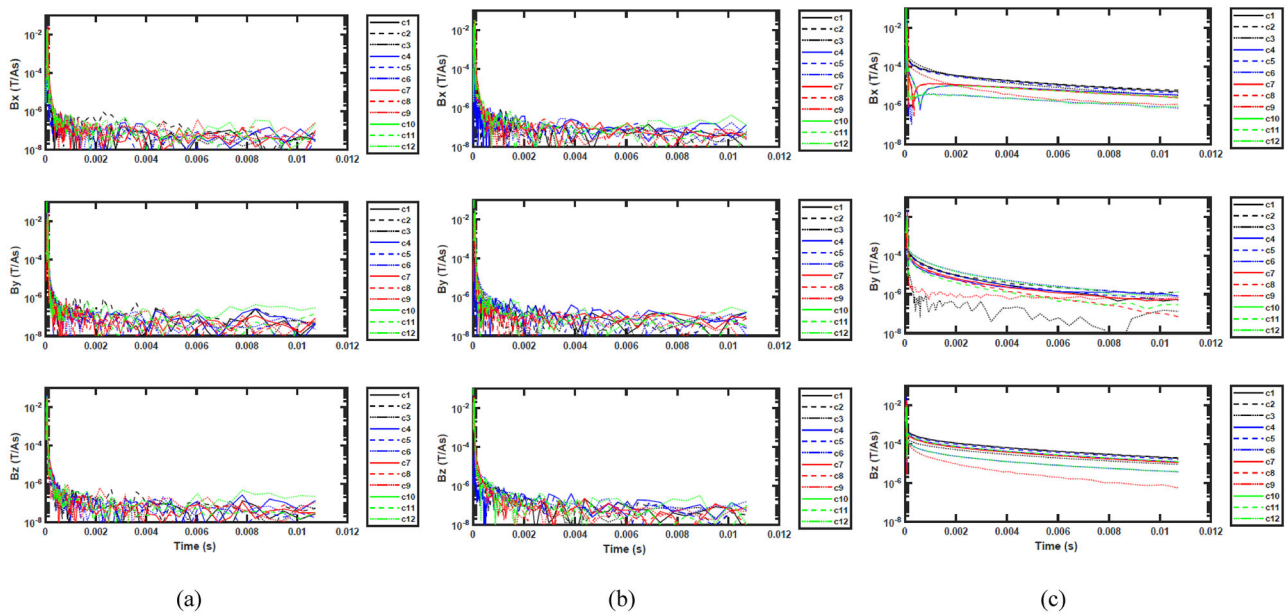

FIGURE 9   (a) Background responses at the test start, (b) background responses at the test end and (c) target response during marine deployment. Each panel represents one transmitter (x, y or z), and responses are measured on 12 channels (c1–c12).
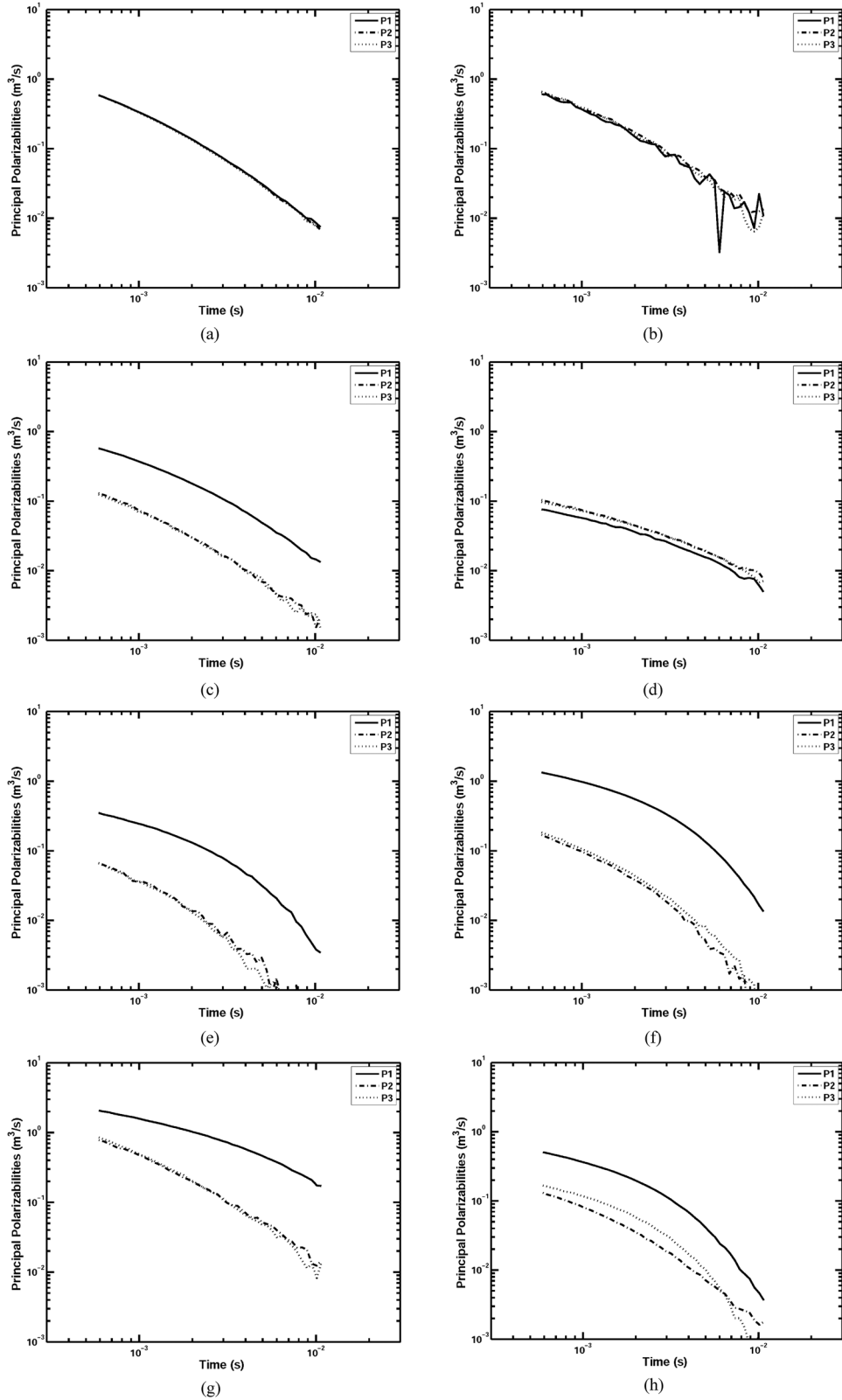
FIGURE 10 Principal polarizabilities as a function of time for test targets: (a) 152-mm shotput, (b) 152-mm shotput at a depth of 1.0 m, (c) 230-mm steel spheroid, (d) 230-mm aluminium spheroid, (e) 60-mm mortar, (f) 70-mm rocket, (g) 105-mm projectile at a depth of 1.0 m at 45° and (h) scrap metal.
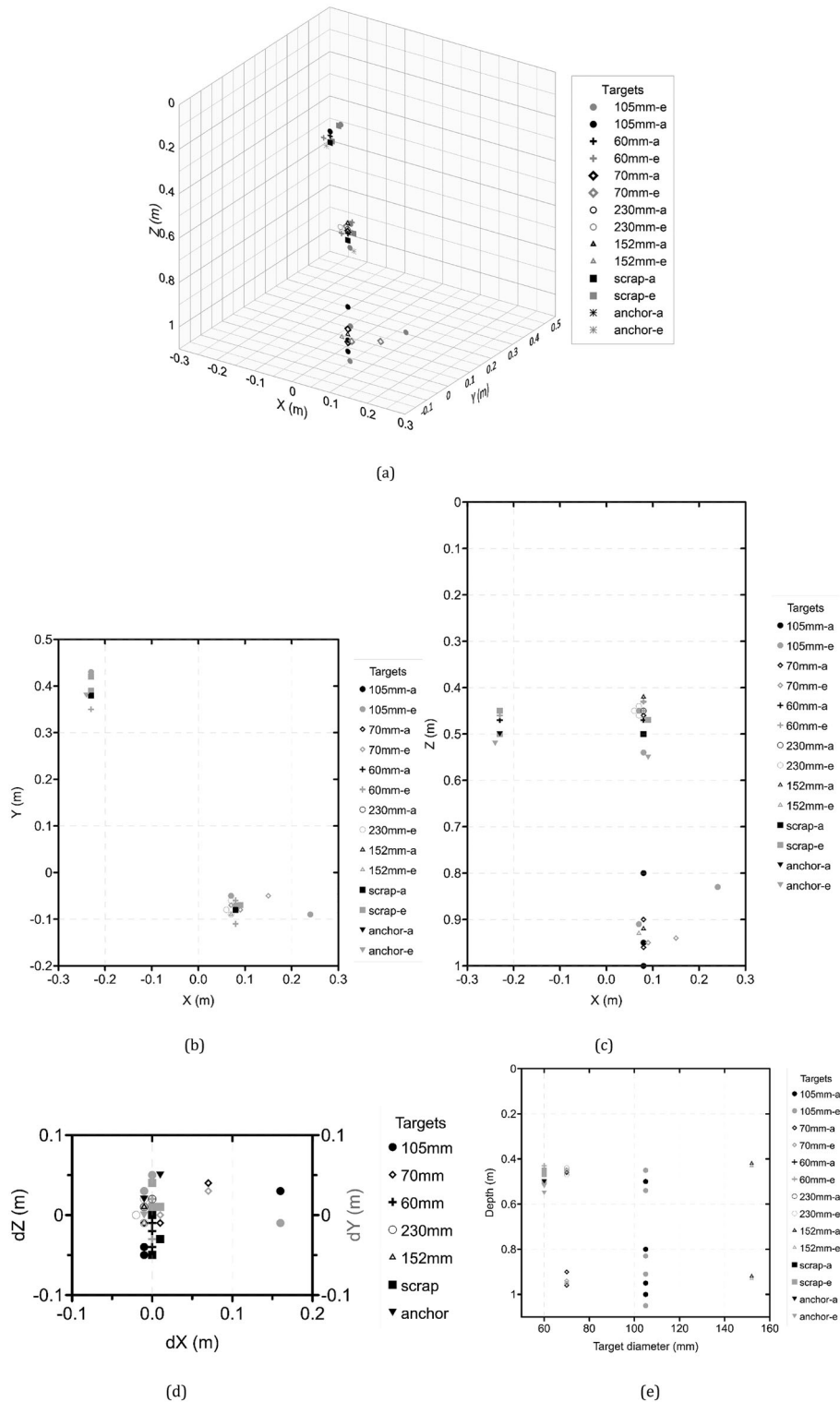
FIGURE 11 Actual (black symbols, a) and estimated (grey symbols, e) object locations in marine experiment. (a) 3D view, (b) *XY* locations, (c) *XZ* locations, (d) differences between actual and estimated values and (e) target depths as a function of a target diameter. Test targets were 105-mm projectile, 60-mm mortar, 70-mm rocket, 230-mm steel and aluminium spheroids, 152-mm shotput, a piece of scrap metal and an anchor.
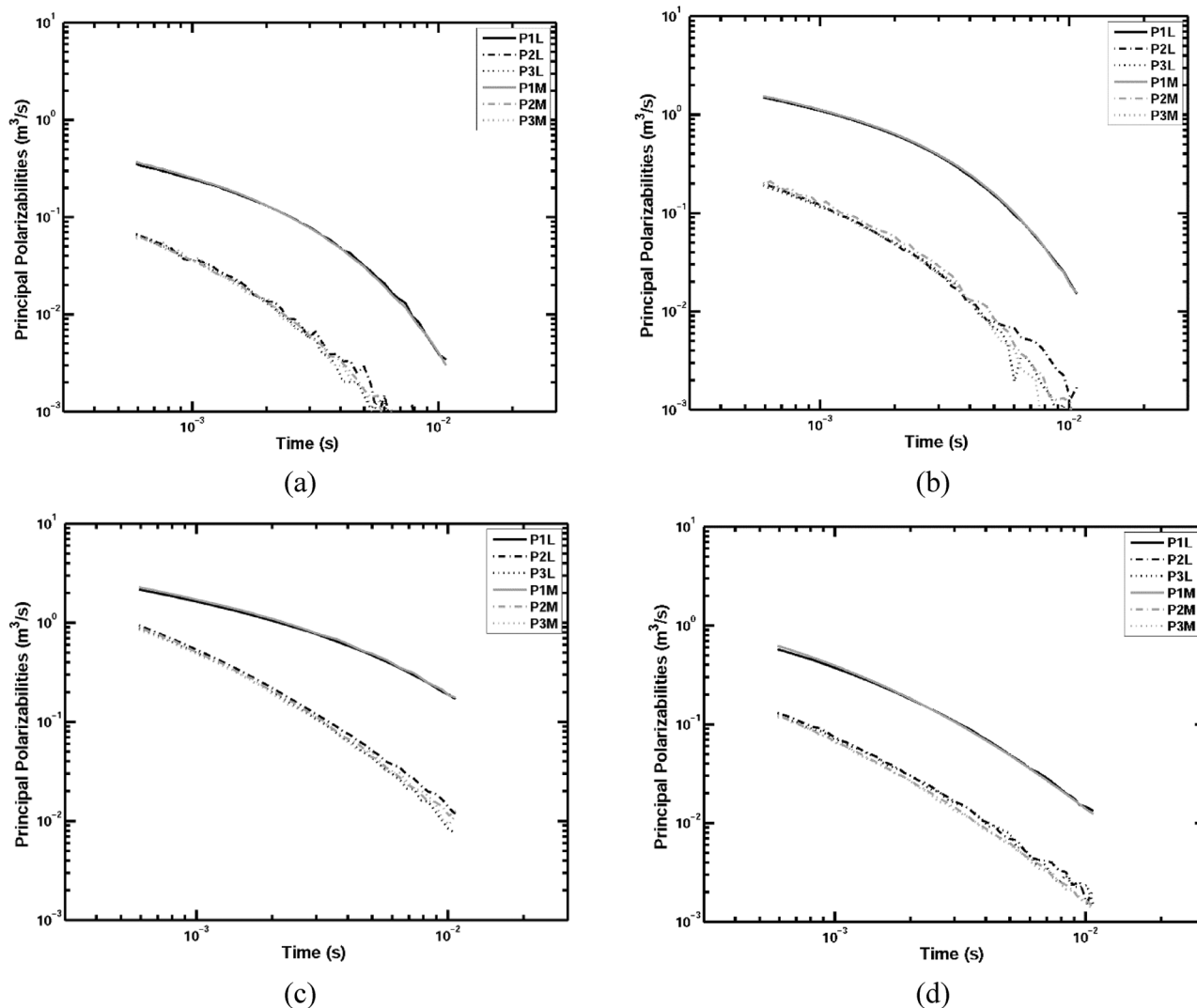
FIGURE 12 Comparison of principal polarizabilities for (a) 60-mm mortar, (b) 70-mm rocket, (c) 105-mm projectile and (d) 230-mm steel spheroid from land (black curves) and underwater tests (grey curves).

air–sea interface is cancelled. The carrier boat used in this experiment is suitable for shallow or deep-water deployments. The acquired data also demonstrated the system's stability and measurement repeatability. The comparison of the underwater and land test results showed that the target responses estimated from marine acquisitions matched those from land measurements. The system can discriminate objects to depths ~10 times the object's diameter, ~1.2 m below the system. The inversion accurately estimates the target's depth, horizontal location and orientation from data in both environments. A unique set of principal polarizabilities characterizes each target. Furthermore, results of 230-mm steel and aluminium spheroids demonstrated that the system can classify objects based on not only their size and shape but also the metal content.

form of this manuscript, or allow others to do so, for U.S. Government purposes.

DISCLAIMER: This document was prepared as an account of work sponsored by the United States Government. While this document is believed to contain correct information, neither the United States Government nor any agency thereof, nor the Regents of the University of California, nor any of their employees, makes any warranty, express or implied, or assumes any legal responsibility for the accuracy, completeness, or usefulness of any information, apparatus, product, or process disclosed, or represents that its use would not infringe privately owned rights. Reference herein to any specific commercial product, process, or service by its trade name, trademark, manufacturer, or otherwise, does not necessarily constitute or imply its endorsement, recommendation, or favoring by the United States Government or any agency thereof, or the Regents of the University of California. The views and opinions of authors expressed herein do not necessarily state or reflect those of the United States Government or any agency thereof or the Regents of the University of California.

DATA AVAILABILITY STATEMENT

Data associated with this research can be obtained from the corresponding author upon reasonable request.

ORCID

Erika Gasperikova https://orcid.org/0000-0003-1553-4569

REFERENCES

Beran, L., Billings, S.D. & Oldenburg, D.W. (2011) Robust Inversion of time-domain electromagnetic data: application to unexploded ordnance discrimination. *Journal of Environmental and Engineering Geophysics*, 16, 127–141. https://doi.org/10.2113/JEEG16.3.127

Beran, L., Zelt, B., Pasion, L., Billings, S., Kingdon, K., Lhomme, N., Song, L.-P. & Oldenburg, D. (2013) Practical strategies for classification of unexploded ordnance. *Geophysics*, 78, E41–E46. https://doi.org/10.1190/geo2012-0236.1

Billings, S.D., Pasion, L.R., Beran, L., Lhomme, N., Song, L.-P., Oldenburg, D.W., Kingdon, K., Sinex, D. & Jacobson, J. (2010) Unexploded ordnance discrimination using magnetic and electromagnetic sensors: case study from a former military site. *Geophysics*, 75, B103–B114. https://doi.org/10.1190/1.3377009

Billings, S. (2020) *UltraTEM marine towed system for detection and characterization of buried ordnance*. Environmental Security Technology Certification Program (ESTCP) Project MR-19-5073. Detection and classification performance report.

Böttcher, C., Knobloch, T., Rühl, N.-P., Sternheim, J., Wichert, U. & Wöhler, J. (2011) Munitionsbelastung der Deutschen Meeresgewässer -Bestandsaufnahme und Empfehlungen (Stand 2011). *Meeresumwelt Aktuell Nord- und Ostsee, 2011/3*. Hamburg, Rostock: Bundesamt für Seeschifffahrt und Hydrographie (BSH).

DiMarco, R., Keiswetter, D. & Bell, T. (2010) *Deep water munitions detection system*. Environmental Security Technology Certification Program (ESTCP) Project MM-0739. Final report.

EPA. (2016) *Uniform federal policy for quality assurance project plans:*. Advanced Geophysical Classification for Munitions Response (AGC-QAPP) Version 1.0. EPA. https://www.epa.gov/fedfac/uniform-federal-policy-quality-assurance-project-plans-template-advanced-geophysical.

Frey, T. (2020) *Quality guideline for offshore explosive ordnance disposal*. Berlin, Wien, Zürich, Beuth Verlag. p. 204.

Funk, R., Gamey, T.J. & Billings, S. (2022) *Ultra TEMA-4 Marine dynamic classification system field trials*. Denver, CO: SAGEEP.

Gasperikova, E., Smith, J.T., Morrison, H.F., Becker, A. & Kappler, K. (2009a). UXO detection and identification based on intrinsic target polarizabilities—a case history. *Geophysics*, 74(1), B1–B8. https://doi.org/10.1190/1.2997419

Gasperikova, E., Smith, J.T., Morrison, H.F. & Becker, A. (2009b) *Demonstration of the Berkeley UXO discriminator at live sites*. Environmental Security Technology Certification Program (ESTCP) Project MR-200838. Demonstration report.

Gasperikova, E., Vytla, V., Jobe, T., Kennedy, L. & Zhu, X. (2012) *Cued survey with a hand-held UXO discriminator at Camp Beale, CA*. Environmental Security Technology Certification Program (ESTCP) Project MR-201166. Demonstration report.

Guldin, D. (2021) Professionelle Kampfmittelräumung—die nächsten Schritte. Überlegungen zur inhaltlichen Neuausrichtung der Kampfmittelräumung offshore und einem neuen technischen Ansatz. In *The Kiel Munitions Clearance Week, 9 September 2021*. Presentation.

Keranen, J., Miller, J.S., Schultz, G., Sander-Olhoeft, M. & Laudato, S. (2018) EMPACT 3D: an advanced EMI discrimination sensor for CONUS and OCONUS applications. *Proc. SPIE 10628, Detection and Sensing of Mines, Explosive Objects, and Obscured Targets XXIII*. p. 106280S. https://doi.org/10.1117/12.2306945

Kulgemeyer, T., Schwartz, M. & Billings, S. (2019) Test of a submarine transient electromagnetic sensor for UXO classification by remotely operated vehicles (SubTEM-ROV). *UACE2019—Conference Proceedings*. pp. 437–442. https://www.uaconferences.org/component/contentbuilder/details/22/102/2019_programme-test-of-a-submarine-transient-electromagnetic-sensor-for-uxo-classification-by-remotely-operated-vehicles-subtem-rov

Miller, J., Schultz, G., Keranen, J. & Shubitidze, F. (2018) Dynamic EMI sensing technologies: developments and demonstrations at live UXO sites on land and underwater. *Fast Times*, 23, 62–69.

Miller, J. (2019) *Underwater dynamic classification technology*. Environmental Security Technology Certification Program (ESTCP) Project MR-201614. *Final report*.

Miller, J., Schultz, G., Keranen, J. & Foley, J. (2021) Dynamic advanced geophysical classification technology. *Symposium on the Application of Geophysics to Engineering and Environmental Problems Proceedings*. pp. 213–213. https://doi.org/10.4133/sageep.33-120

Morrison, H.F. (2013) *Development and testing of an engineering prototype for a marine version of the Berkeley Unexploded Ordnance Discriminator (BUD)*. Strategic Environmental Research and Development Program (SERDP) Project MR-2228. Final report.

Pasion, L.R., Billings, S.D., Oldenburg, D.W. & Walker, S.E. (2007) Application of a library based method to time domain electromagnetic data for the identification of unexploded ordnance. *Journal of Applied Geophysics*, 61, 279–291.

Prouty, M., George, D.C., Snyder, D.D. (2011) *MetalMapper: a multisensory TEM system for UXO detection and classification*. Environmental Security Technology Certification Program (ESTCP) Project MR-200603. Final report.

Schultz, G. (2016) *Demonstration of ROV-based underwater electromagnetic array technology*. Environmental Security Technology Certification Program (ESTCP) Project MR-201233. Final report.

Schultz, G., Miller, J., Keranen, J. & Shubitidze, F. (2021) ROV-based 3D-controlled source electromagnetics for UXO detection and classification. In *Symposium on the Application of Geophysics to Engineering and Environmental Problems Proceedings*: pp. 346–346. https://doi.org/10.4133/sageep.33-191

Shubitidze, F., Fernandez, J.P., Barrowes, B.E., Shamatava, I., Bijamov, A., O'neill, K., Karkashadze, D. (2014) The orthonormalized volume magnetic source model for discrimination of unexploded ordnance. *IEEE Transactions on Geoscience and Remote Sensing*, 52, 4658–4670.

Shubitidze, F., Barrowes, B., Keranen, J., Miller, J. & Shamatava, I. (2021a) Fast and accurate detection and classification subsurface targets using emerging sensors' data sets. *Symposium on the Application of Geophysics to Engineering and Environmental Problems Proceedings*. pp. 215–215. https://doi.org/10.4133/sageep.33-122

Shubitidze, F., Barrowes, B., Maxson, M.L. & Shamatava, I. (2021b) Time domain EMI responses for multilayer structure to enhance underwater UXO detection and classification. *Symposium on the Application of Geophysics to Engineering and Environmental Problems Proceedings*. pp. 349–349. https://doi.org/10.4133/sageep.33-194

Smith, J.T. & Morrison, H.F. (2004) Estimating equivalent dipole polarizabilities for the inductive response of isolated conductive bodies. *IEEE Transactions on Geoscience and Remote Sensing*, 42, 1208–1214.

Song, L.-P., Oldenburg, D.W. & Pasion, L.R. (2012) Estimating source locations of unexploded ordnance using the multiple signal classification algorithm. *Geophysics*, 77, WB127–WB135. https://doi.org/10.1190/geo2011-0379.1

Song, L.-P., Billings, S.D., Pasion, L.R. & Beran, L. (2021) Modeling and characterizing EMI response in a multilayered marine munitions site. *Symposium on the Application of Geophysics to Engineering and Environmental Problems Proceedings*. pp. 344–344. https://doi.org/10.4133/sageep.33-189

Wehner, D. & Frey, T. (2022) Offshore unexploded ordnance detection and data quality control—a guideline. *IEEE Journal of Selected Topics in Applied Earth Observations and Remote Sensing*, 15, 7483–7498. https://doi.org/10.1109/JSTARS.2022.3200144